HHS Public Access

Author manuscript

FASEB J. Author manuscript; available in PMC 2021 January 01.

Published in final edited form as:

FASEB J. 2020 January ; 34(1): 148–160. doi:10.1096/fj.201900751R.

Intraflagellar-transport A dysfunction causes hyperphagia-induced systemic insulin resistance in a pre-obese state

Damon T Jacobs[*], **Bailey A Allard**[*], **Tana S Pottorf**, **Luciane M Silva**, **Wei Wang**, **Aisha Al-Naamani**, **Ewud Agborbesong**, **Tao Wang**, **Dajanae A Carr**, **Pamela V Tran**

[1]Dept. of Anatomy and Cell Biology, Jared Grantham Kidney Institute, University of Kansas Medical Center, Kansas City, KS

Abstract

Deletion of murine *Thm1*, an intraflagellar transport A (IFT-A) component that mediates ciliary protein trafficking, causes hyperphagia, obesity and metabolic syndrome. The role of *Thm1* or IFT-A in adipogenesis and insulin sensitivity is unknown. Here we report that *Thm1* knock-down in 3T3–L1 pre-adipocytes promotes adipogenesis and enhances insulin sensitivity *in vitro*. Yet pre-obese *Thm1* conditional knock-out mice show systemic insulin resistance. While insulin-induced AKT activation in *Thm1* mutant adipose depots and skeletal muscle are similar to those of control littermates, an attenuated insulin response arises in the mutant liver. Insulin treatment of control and *Thm1* mutant primary hepatocytes results in similar AKT activation. Moreover, pair-feeding *Thm1* conditional knock-out mice produces a normal insulin response, both in the liver and systemically. Thus, hyperphagia caused by a cilia defect, induces hepatic insulin resistance via a non-cell autonomous mechanism. In turn, hepatic insulin resistance drives systemic insulin resistance prior to an obese phenotype. These data demonstrate that insulin signaling across cell types is regulated differentially, and that the liver is particularly susceptible to hyperphagia-induced insulin resistance and a critical determinant of systemic insulin resistance.

Keywords

primary cilia; mouse model; adipogenesis; metabolism; liver

Introduction

Obesity affects 1 in 3 individuals worldwide and associates with insulin resistance, placing individuals at heightened health risk. Adipose tissue plays a critical role in insulin sensitivity and serves both as an energy depot and endocrine organ (1). In the latter role, adipose tissue secretes adipokines that are received by multiple organs, including the brain, liver, skeletal muscle and pancreas, regulating systemic energy homeostasis. Expansion of adipose tissue

Correspondence should be addressed to: Pamela V. Tran, Department of Anatomy and Cell Biology and The Jared Grantham Kidney Institute, University of Kansas Medical Center, 3901 Rainbow Blvd., MS #3038, Kansas City, KS 66160, Tel: 913-945-7325, Fax: 913-588-2710, ptran@kumc.edu.

[*]First co-authorship

Author Contributions

BAA, DTJ, TSP, LMS, WW, AA, EA, TW, DAC and PVT performed experiments and analyzed data. DTJ, BAA and PVT designed research. AA contributed new reagents. AA, BAA and PVT wrote the paper.

can result from hypertrophy, which is the enlargement of adipocytes, or hyperplasia, which is the increased formation of adipocytes from precursor cells. While hypertrophy is associated with adipocytes with metabolic dysfunction, formation of new adipocytes from pre-adipocytes may promote healthy metabolism (1–3).

Genetic disorders, which manifest obesity and metabolic dysfunction, can provide valuable insights into underlying cellular and molecular mechanisms. Such disorders include ciliopathies caused by defects in primary cilia, which are antenna-like sensory organelles that mediate signaling pathways (4). Since most vertebrate cells have a primary cilium, ciliopathies manifest multiple clinical features, including renal, hepatic and pancreatic cystic diseases, retinal degeneration, and skeletal, neural and craniofacial defects. Additionally, in two ciliopathies, Alström Syndrome and Bardet-Biedl Syndrome (BBS), obesity presents as a central clinical feature, linking obesogenic processes to ciliary dysfunction (5, 6).

Intraflagellar transport (IFT) or the bi-directional transport of protein cargo along a microtubular axoneme is essential to cilia synthesis and maintenance (7, 8). The IFT-B complex associates with the kinesin-2 motor, which mediates anterograde IFT from the ciliary base to the tip, and the IFT-A complex and the cytoplasmic dynein motor mediate retrograde IFT from the ciliary tip to the base. IFT-A proteins also regulate ciliary entry of signaling and membrane-associated proteins in mammalian cells (9, 10). Other ciliary protein complexes include the BBSome, which acts as an adaptor between IFT complexes and protein cargo, transporting signaling molecules to and throughout the cilium (11–15), and the BBS-chaperonin complex, which facilitates BBSome formation (16, 17).

Primary cilia present on confluent pre-adipocytes, lengthen during early differentiation, then shorten during later differentiation stages and are absent in mature, lipid-filled adipocytes (18). Knock-down of Ift-B component, *Ift88*, of kinesin subunit, *Kif3a*, or of *Alms1*, which is mutated in Alström Syndrome, inhibits differentiation of 3T3–L1 mouse pre-adipocytes (19, 20). In contrast, patient-derived fibroblasts with mutations in the BBS-chaperonin components, *BBS10* and *BBS12*, and *BBS12*-deficient human primary mesenchymal stem cells show enhanced adipogenesis. Further, obese *Bbs12* knock-out mice have heightened adipose insulin sensitivity and enhanced systemic glucose and insulin metabolism, consistent with the notion that adipogenesis benefits metabolism (21, 22). Yet, lean, calorie-restricted mice null for *Bbs4*, a component of the BBSome, are insulin-resistant (23). These opposing phenotypes indicate complexity in the regulation of adipogenesis and metabolic health by ciliary proteins.

The role of IFT-A in adipogenesis has not been reported. Mutations of IFT-A gene, *THM1* (*TPR-containing Hedgehog Modulator 1*; also known as *TTC21B*) (24), have been identified in BBS patients (25). Consistent with a role for *THM1* in BBS, deletion of *Thm1* in adult mice causes hyperphagia and obesity, which is preceded by misregulation of *Pomc1* and *Npy* appetite-controlling neuropeptides (26). To investigate additional underlying mechanisms of *Thm1*-deficient metabolic disease, here we examine the role of *Thm1* in adipogenesis and insulin resistance. Our findings demonstrate that diminished *Thm1* levels in pre-adipocytes enhances insulin sensitivity and promotes adipogenesis *in vitro*. Yet pre-obese *Thm1* conditional knock-out (cko) mice show systemic insulin resistance and an

attenuated insulin response in hepatic tissue. Control- and *Thm1* cko-derived primary hepatocytes have similar insulin sensitivity. Moreover, pair-feeding *Thm1* cko mice produces a normal insulin response. These data reveal that hyperphagia caused by defective cilia drives insulin resistance prior to an obese phenotype in a non cell-autonomous manner. Additionally, these data reveal that the liver is particularly sensitive to hyperphagia-induced insulin resistance and an important determinant of systemic insulin resistance, and in turn, metabolic disease.

Materials and Methods

Generation of Thm1 kd 3T3–L1 cell lines

3T3–L1 mouse preadipocytes (ATCC; CL-173) were maintained in the pre-adipocyte state by culturing in pre-adipocyte expansion media, consisting of 90% Dulbecco's Modified Eagle's Medium DMEM (ATCC, 30–2002), 10% Bovine Calf Serum (ATCC, 30–2030) and 1% penicillin/streptomycin, and passaging cells at 70% confluency.

To knock down *Thm1*, lentiviruses expressing *Thm1* shRNA were generated as described (24). Briefly, pLKO.1 (empty vector or EV for control) or pLKO.1-*Thm1* 5'-GTTCGTAGATGCCATTGAA-3', together with delta 8.2 and VSVG plasmids, were transfected into 293T packaging cells using Viafect Transfection Reagent according to manufacturer's instructions (Promega). Forty-eight hours after transfection, supernatant containing virus was collected and filtered. 3T3–L1 cells were infected with virus for 4 hours. Infected cells were selected with 1μg/ml puromycin. Cells were plated sparsely to allow individual clones to form. Clones of 50–100 cells were picked using cloning disks (VWR) immersed in Trypsin, and expanded.

Differentiation Assay

Cells were differentiated according to ATCC's chemically-induced differentiation protocol. Cells were plated in pre-adipocyte expansion media. Two days post-100% confluency is designated as Differentiation Day 0 (DD0). From DD0 until DD2, cells continued to be cultured in pre-adipocyte expansion media. On DD2, media was replaced with adipocyte expansion media, containing DMEM (ATCC), 10% Fetal Bovine Serum (Sigma), 1% penicillin/streptomycin, 1.0 μM dexamethasone (Sigma), 0.5 mM methylisobutylxanthine (IBMX; Sigma) and 1.0 μg insulin (Sigma). On DD5, adipocyte expansion media was replaced with adipocyte maintenance media, containing DMEM (ATCC), 10% FBS, 1% penicillin/streptomycin and 1.0μg insulin (Sigma) until DD8.

Oil Red O Staining

3T3–L1 empty vector (EV) and *Thm1* knock-down (kd) cells were seeded onto poly-L-lysine coated coverslips in a 24-well plate and differentiated. At DD8, cells were fixed with 4% paraformaldehyde in phosphate-buffered saline for 1 hour. Cells were then incubated with 60% isopropanol for 5 minutes and subsequently stained with Oil Red O (Sigma) for 20 minutes. After removing Oil Red O stain, cells were counterstained with hematoxylin (Sigma) for 20 seconds, then rinsed. Coverslips were inverted and mounted with Fluoromount-GT (Electron Microscopy Sciences) onto a slide.

Immunofluorescence Staining

Cells were seeded onto Poly-L-Lysine coated coverslips in 24-well plates. At desired experimental time points, cells were fixed with 4% paraformaldehyde in phosphate-buffered saline containing 0.1% Triton x-100 for 10 minutes at room temperature. Cells were blocked in 2% Bovine Serum Albumin (Sigma) for 1 hour at room temperature. Cells were then incubated with primary antibody diluted in blocking solution overnight at 4°C. Primary antibodies used include: acetylated alpha-tubulin (Sigma), ARL13B (Proteintech), IFT-81 (Proteintech), γ-tubulin (Sigma), PPARγ (Cell Signaling), and CEBPα (Cell Signaling). Cells were washed and incubated with secondary antibody, AF488 or AF542 (Life Technologies) for 1 hour at room temperature. To visualize lipid droplets, slides were incubated with BODIPY (Fisher) for one hour at room temperature. Coverslips were inverted and mounted onto slides using DAPI Fluoromount-G (Electron Microscopy Services, 17984–24). Cells were visualized and imaged using a Nikon80i microscope attached to a Nikon DS-Fi1 camera.

Protein Extraction and Western Blot

Protein from cells and tissue was extracted using Passive Lysis Buffer (Promega) with protease/phosphatase inhibitor mini tablets, EDTA free (Pierce). Cells were resuspended and rocked in lysis buffer for 15 minutes, centrifuged at maximum speed for 1 minute. Supernatants were then collected. Frozen tissue was homogenized in lysis buffer using Bullet Blender Bead Lysis tubes (MidSci) and a Bullet Blender Storm 24 (Next Advance) set at Speed 10 for approximately 10 minutes. Homogenates were centrifuged at 4°C at maximum speed for 1 minute, and supernatants were collected. Protein concentration was determined using the BCA assay (Pierce). Cell and tissue protein extracts (35–40μg protein/lane) were loaded onto a 4–20% SDS-gel (BioRad). Proteins were transferred onto PVDF membrane (Millipore). Membranes were incubated in blocking solution (5% milk in TBST). Membranes were incubated with primary antibodies: THM1 (Sigma), phosphorylated AKT (Cell Signaling), phosphorylated ERK (Cell Signaling), AKT (Cell Signaling), ERK (Cell Signaling), ß-Actin (Cell Signaling), PPARγ (Cell Signaling), and CEBPα (Cell Signaling) overnight at 4°C. Membranes were washed and incubated with secondary antibodies conjugated to HRP (Cell Signaling). Signal was detected using SuperSignal West Femto Maximum Sensitivity Substrate (Pierce) and imaged using an Amersham Imager 600.

Insulin treatment and tissue retrieval from Thm1 conditional knock-out mouse

All animal procedures were approved by the Institutional Animal Care and Use Committee at University of Kansas Medical Center. *Thm1* conditional knock-out mice on a mixed FVB/C57BL/6J strain background were generated and maintained using *Thm1* floxed alleles, $Thm1^{aln}$ (null) allele and the $Rosa26\text{-}Cre^{ERT}$ allele (Jackson Laboratory) as described (26). $Thm1^{fl/aln}$; $Rosa26\text{-}Cre^{ERT}$ mice and control littermates were injected intraperitoneally with 10mg/40g tamoxifen (Sigma) at 5 weeks of age. *Ad libitum* fed pre-obese or overweight *Thm1* conditional knock-out mice ($Thm1^{fl/aln}$; $Rosa26\text{-}Cre^{ERT}$) at two or seven weeks post-*Thm1* deletion, respectively (26), were fasted overnight, then injected intraperitoneally with 5U/kg insulin (Sigma). Thirty minutes after insulin injection, mice were euthanized and tissues were collected and snap-frozen. A cohort of *Thm1* conditional knock-out mice were

individually housed following *Thm1* deletion and pair-fed for two weeks. Pair-fed mice were then fasted and treated with insulin in the same manner as *ad libitum* fed mice.

Insulin tolerance test

Following a 5-hour fast, mice were administered insulin (0.75U/kg or 0.25U/kg; Sigma) intraperitoneally, and glucose measurements from tail blood were taken using a Bayer Contour Blood Glucose monitor at 15-minute intervals from 0 to 60 minutes following insulin injection.

Mouse Primary Hepatocyte Isolation

Primary hepatocytes were isolated from mice using a two-step collagenase perfusion method as described previously(27, 28). Following anesthesia with ketamine and xylazine, the liver was perfused via the inferior vena cava for 10 min at 37°C first with calcium- and magnesium-free Hank's Balanced Salt Solution (HBSS; Hyclone), then with HBSS containing calcium and magnesium (Hyclone) and 0.025mg/ml of Liberase TM (Roche). Once the liver revealed signs of digestion (approximately 8–10 minutes), the liver was excised and minced in cold calcium- and magnesium-free HBSS. The cell suspension was filtered through a nylon gauze (100 μm) and collected in 50 ml conical tubes. The cells were centrifuged for 5 minutes at 50 rcf at 4°C, then resuspended in fresh cold calcium- and magnesium-free HBSS. This was repeated 3 times to isolate the hepatocyte fraction. Hepatocyte viability was evaluated using the trypan blue exclusion method and number of hepatocytes was determined using a haemocytometer.

Primary Hepatocyte Insulin Treatment

Primary hepatocytes (6×10^5cells/well) were cultured in a 6-well plate in Williams E media overnight. The following morning, cells were treated with 10nM or 100nM insulin for 5 minutes. Cells were washed in PBS, then pelleted and stored at −20°C until protein extraction.

Results

Thm1 deficiency promotes adipogenesis

3T3–L1 pre-adipocytes were infected with lentiviruses expressing *Thm1* shRNA and clonally selected. Western blot analysis of *Thm1* knock-down (kd) clones revealed up to 80% reduction in THM1 levels (Figure 1A). In *Thm1* kd cells, immunostaining for ARL13B, a ciliary membrane protein, revealed shorter ciliary length, while immunostaining for IFT81, a marker of the ciliary axoneme, revealed accumulation of this protein in bulbous distal tips indicative of defective retrograde IFT (Figure 1B). Statistically significant differences between control (EV – empty vector) and *Thm1* kd ciliary lengths was achieved using ARL13B, but not IFT81. This could be because IFT81 accumulation in ciliary distal tips of *Thm1* kd cells may cause staining beyond the ciliary axoneme, whereas IFT81 labeling may be more restricted to the axonemes in control cells. Overall, the ciliary mutant phenotype is consistent with an IFT-A defect (24).

We next examined capacity of *Thm1* kd pre-adipocytes to form mature adipocytes. Differentiation into mature adipocytes was determined on DD8 by staining lipid droplets with Oil Red O. *Thm1* kd clones showed markedly increased Oil Red O staining relative to control cell lines, indicating enhanced adipogenesis (Figure 1C).

PPARγ and C/EBPα are increased in *Thm1*-deficient cells by early differentiation

The differentiation of pre-adipocytes into mature adipocytes is orchestrated by downregulating Wnt and Hedgehog (Hh) signaling pathways, and activating insulin signaling, leading to expression of adipocyte master transcriptional regulators, Caat/Enhancer Binding Protein alpha (CEBPα) and Peroxisome proliferator-activated receptor gamma (PPARγ). Using Western blot, we analyzed levels of THM1, PPARγ, CEBPα and CEBPß, at various time points from 70% confluency to DD8. At all differentiation states, THM1 levels remained low in *Thm1* kd cells (Figure 2A; Figure S1). By DD5, PPARγ, CEBPα and CEBPß levels were higher in *Thm1* kd cells than in EV cells, and at DD8, these transcription factors were even more elevated in *Thm1* kd cells relative to EV cells. We immunostained cells for PPARγ and C/EBPα together with incubating with boron-dipyrromethene (BODIPY), a fluorescent dye with affinity to lipids. *Thm1* kd cells showed increased nuclear staining of PPARγ and C/EBPα relative to control cells as early as DD1 (Figure 2B). At this early differentiation stage, lipid droplets have not yet formed, as shown by absence of BODIPY stain. At DD8, *Thm1* kd cells continue to show greater nuclear C/EBPα and PPARγ expression than control cells. BODIPY-stained lipid droplets are present in both control and *Thm1* kd cells, but are more abundant in *Thm1* kd cells. Together, these data indicate that *Thm1* deficiency in pre-adipocytes increases the propensity of cells to differentiate.

Thm1 kd pre-adipocytes potentiate insulin signaling

We next examined the Hedgehog (Hh) signaling pathway, which is downregulated during differentiation of pre-adipocytes. Using qPCR, extracts of *Thm1* kd pre-adipocytes at DD0 showed elevated *Gli1* and *Gli2* transcripts and decreased *Gli3* transcripts, suggesting *Thm1* deficiency causes upregulation of the Hh pathway at DD0 (Figure 3A). We next examined capacity of cells at DD0 to respond to insulin, which is essential for pre-adipocyte differentiation and activates AKT and ERK. Control and *Thm1* kd preadipocytes at DD0 were treated with 100nM insulin for various durations. *Thm1* kd cells showed greater P-AKT/AKT and P-ERK/ERK ratios in response to insulin than control cells (Figure 3B; Figure S2), indicating increased insulin sensitivity. We also examined adipogenesis in the absence of one of three components that are critical in the differentiation media. These components include: dexamethasone (DEX), a glucocorticoid agonist that drives expression of PPARγ; methylisobutylxanthine (IBMX), which stimulates cAMP; and insulin. Omission of either DEX or IBMX from the differentiation media hindered adipogenesis of both control and *Thm1* kd cells (Figure S3). In contrast, absence of insulin from the differentiation media reduced adipogenesis in control cells, but only slightly in *Thm1* kd cells, suggesting the *Thm1* kd cells are more resilient to the absence of insulin. These data suggest that *Thm1* deficiency in pre-adipocytes potentiates insulin signaling.

Pre-obese *Thm1* conditional knock-out mice show systemic insulin resistance

Since hyperplasia in adipose tissue may promote healthy metabolism (1–3), increased differentiation of *Thm1*-deficient pre-adipocytes has potential to enhance insulin sensitivity and metabolic health. For instance, *BBS12*-patient derived fibroblasts and *BBS12*-deficient mesenchymal stem cells show enhanced adipogenesis and *Bbs12* knock-out mice have heightened systemic insulin sensitivity (22). We reasoned that analysis of pre-obese mice would best reveal the direct role of *Thm1* deficiency on metabolism; whereas metabolic changes in obese animals can be secondary, since disease processes have already taken place. We deleted *Thm1* globally in mice at 5 weeks of age using the tamoxifen-inducible *ROSA26*-Cre^{ERT} recombinase. Previously, we observed that *Thm1* conditional knock-out (cko) mice begin to show increased body weight relative to control littermates at three weeks following gene deletion (26). Therefore, two weeks following gene deletion and prior to an obese phenotype (Figure S3), we examined insulin sensitivity in *Thm1* cko mice. In response to an i.p. injection of insulin at a dose of 0.75U/kg, pre-obese *Thm1* cko mice and control littermates showed similar glucose clearance (Figure 4A). Since deficiency of *BBS12* enhances adipogenesis and heightens systemic insulin sensitivity (22), we questioned whether a lower insulin dose would reveal differences in insulin sensitivity between control and *Thm1* cko mice. In response to an insulin dose of 0.25U/kg, glucose levels in control mice continued to decrease at 45 minutes post-insulin administration. However, glucose levels in pre-obese *Thm1* cko mice decreased until 30 minutes post-insulin administration, and were significantly increased at 45 minutes post-insulin administration relative to glucose levels in control mice (Figures 4B–D). Thus, in contrast to *Bbs12* knock-out mice, pre-obese *Thm1* cko mice have systemic insulin resistance.

Insulin-induced AKT activation is attenuated in liver of pre-obese *Thm1* conditional knock-out mice

To determine the origin of this systemic insulin resistance, we examined AKT activation in gonadal and mesenteric adipose depots, skeletal muscle and liver, in response to an intraperitoneal injection of insulin. Insulin activated AKT (P-AKT/AKT ratios) in gonadal and mesenteric adipose depots and in skeletal muscle of pre-obese *Thm1* cko and control mice similarly (Figures 5A–C). However, in liver of pre-obese *Thm1* cko mice, insulin did not activate AKT (Figure 5D).

We next assessed insulin response in overweight *Thm1* cko mice at 7 weeks following gene deletion (Figure S4). Following insulin injection (0.25U/kg), glucose levels in mutant mice reduced very minimally or not at all (Figures 6A–C). Additionally, at each time point, glucose levels in mutant mice were significantly elevated relative to control littermates, indicating that the systemic insulin resistance worsens with time following gene deletion. Moreover, while insulin administration to overweight *Thm1* cko mice activated AKT in gonadal adipose tissue (Figure 7A), AKT was not activated in mesenteric adipose tissue, skeletal muscle nor liver (Figures 7B–D). These data indicate that insulin resistance is evident first in the liver, then in mesenteric adipose tissue and skeletal muscle. In contrast, gonadal adipose tissue is not affected by insulin resistance in overweight *Thm1* cko mice.

Cultured *Thm1*-mutant primary hepatocytes and pair-fed *Thm1* conditional knock-out mice show normal insulin response

To determine if the insulin resistance in the liver is a direct effect of *Thm1* deletion, we isolated primary hepatocytes from pre-obese *Thm1* cko mice and littermate controls and examined insulin response in cultured cells. Primary hepatocytes of control and *Thm1* cko mice showed similar levels of insulin-induced AKT activation (Figure 8A), suggesting the hepatic insulin resistance observed *in vivo* is an indirect effect of *Thm1* deficiency. To determine if hyperphagia in *Thm1* cko mice (26) may be a factor in inducing insulin resistance, we pair-fed the animals for two weeks following *Thm1* deletion. This time point coincides with the juncture at which *ad libitum*-fed pre-obese mice were examined. Pair-fed *Thm1* cko mice responded similarly to control littermates in an insulin tolerance test (Figure 8B). Further, i.p. administration of insulin caused similar AKT activation in the livers of control and pair-fed *Thm1* cko mice (Figure 8C). These data reveal that hyperphagia drives the hepatic insulin resistance, which in turn, drives the systemic insulin resistance.

Discussion

In this study, we demonstrate the role of IFT-A in adipogenesis and insulin sensitivity. *Thm1* deficiency in 3T3–L1 pre-adipocytes promotes insulin signaling and adipogenesis. This is similar to *BBS10*- and *BBS12*-mutant fibroblasts, but contrasts with IFT-B deficiency in 3T3–L1 pre-adipocytes, which suppresses adipogenesis and decreases insulin sensitivity (19, 29). These differences likely reflect that ciliary proteins work in concert to tune anti- and pro-adipogenic signaling pathways. For instance, the cilium intricately regulates the Hh pathway; Hh signaling components enrich in the cilium to enable pathway transduction, and IFT-B and –A proteins act as positive or negative Hh modulators in a context-dependent manner (8). Similarly, insulin signaling may be fine-tuned at the cilium. In support of this, insulin-signaling components, IGF1Rβ, P-IRS and P-AKT, have been shown to localize to primary cilia or basal bodies of 3T3–L1 pre-adipocytes in response to insulin (29, 30). Additionally, the insulin receptor has been localized to primary cilia of insulin-stimulated β cells of the pancreas (31).

Although *Thm1* deficient pre-adipocytes are sensitized to insulin signaling *in vitro*, pre-obese *Thm1* cko mice show systemic insulin resistance, and insulin response is first attenuated in the liver. Yet primary hepatocytes derived from control and *Thm1* cko mice have similar insulin response, suggesting the hepatic insulin resistance *in vivo* is not a direct effect of *Thm1* deletion and arises from a non-cell autonomous mechanism. Moreover, pair-feeding *Thm1* cko mice produces a normal insulin response, supporting that differences between *in vitro* and *in vivo* (*ad libitum* fed mutant mice) insulin sensitivity may reflect cell autonomous versus non-cell autonomous effects, respectively. Ultimately, these data indicate that hepatic insulin resistance is driven by hyperphagia caused by defective cilia, and in turn, hepatic insulin resistance drives systemic insulin resistance. Interestingly, the liver is also the primary organ in diet-induced insulin resistance (32, 33). Thus, our data reveal convergence between cilia- and diet-induced insulin resistance mechanisms. The mechanisms which give rise to the particular susceptibility of the liver to hyperphagia-induced insulin resistance remain to be explored.

In overweight mutants, insulin-induced AKT activation was attenuated not only in the liver, but also in skeletal muscle and mesenteric adipose tissue, revealing a timeline by which various tissues are affected with insulin resistance in a cilia model. In contrast to these affected tissues, gonadal adipose tissue continued to show robust insulin-induced AKT activation. This may be due to the increased propensity of *Thm1*-deficient pre-adipocytes to differentiate into mature adipocytes. However, the difference in insulin sensitivity between mesenteric and gonadal adipose depots may reflect that the context in which pre-adipocytes are situated may affect differentiation due to non-cell autonomous effects. Pre-adipocytes in mesenteric adipose tissue may encounter more factors that negatively regulate adipogenesis than pre-adipocytes in gonadal adipose depots. Our findings demonstrate that insulin signaling is regulated differentially across tissues, consistent with previous reporting that not all insulin signaling defects equally impact, for instance, the liver and muscle (34–36).

Intriguingly, primary cilia are not present on all insulin-responsive cells. Pre-adipocytes have primary cilia, while mature adipocytes do not (18). Similarly, hepatoblasts, which are present during embryogenesis, have primary cilia, but differentiated hepatocytes in the adult liver do not (37, 38). This raises the questions: Do ciliary proteins regulate insulin signaling outside the cilium? Is insulin signaling regulated differentially between ciliated and non-ciliated cells? An extra-ciliary role for BBS proteins in intracellular trafficking of the insulin receptor was demonstrated by reduced levels of insulin receptor at the cell surface in *Bbs1*- or *Bbs2*-deficient HEK293T cells (23). Additionally, IFT proteins have been shown to enable proper formation and signaling at the immune synapse between a T-cell and an APC cell, both of which lack primary cilia (39). Thus, in cells lacking primary cilia, IFT proteins may generate signaling centers in alternative compartments.

Previously, we demonstrated that *Thm1* cko mice are hyperphagic and that gene expression of appetite-controlling neuropeptides is misregulated prior to obesity onset (26). Our *in vitro* studies here suggest increased adipogenesis may be an additional mechanism underlying *Thm1*-deficient obesity. The enhanced adipogenesis in *Thm1*, *Bbs10* and *Bbs12* mutant cells suggests possible common mechanisms between these individual ciliary proteins or possibly between IFT-A and BBS-chaperonin complexes. Our data add to the known cellular and molecular processes that drive adipose tissue hyperplasia. Since adipose hyperplasia can promote healthy metabolism (1), knowledge of these processes can help identify novel therapeutic targets against insulin resistance (34). However, we also demonstrate that *Thm1* deficiency causes hyperphagia-induced insulin resistance prior to an obese phenotype in a non-cell autonomous manner. Thus, while *Thm1* deficiency may be advantageous in some cell types, it is disadvantageous in others. This, together with our data demonstrating that insulin signaling is regulated differentially across cell types, highlights the importance of increasing our understanding of insulin signaling in various contexts. Finally, our data provide a chronology of tissues affected by insulin resistance in a cilia model and suggest that *THM1* mutations likely modify insulin sensitivity in BBS patients harboring *THM1* and *BBS* mutant alleles (25). Beyond BBS and ciliopathies, the presence of *BBS* polymorphisms in obese individuals in the general population (40), and the occurrence of aberrant cilia dynamics in adipose-derived mesenchymal stem cells from obese individuals in the general population (41) indicate an increasingly widespread relevance for cilia-mediated mechanisms.

Supplementary Material

Refer to Web version on PubMed Central for supplementary material.

Acknowledgements

We thank members of the KUMC Department of Anatomy and Cell Biology, the Jared Grantham Kidney Institute and the Metabolism Group for helpful discussions. We also thank the KUMC Liver Center Cell Isolation Core, which is supported by the National Institutes of Health [P30GM118247]. This work was also supported by the Department of Education, GEAR UP Washington Cluster [DED0068469 to DC], and by the National Institutes of Health [K-INBRE P20GM103418]; [P30DK106912 to BAA]; [R01DK103033 to PVT].

Nonstandard Abbreviations

ARL13B	ADP Ribosylation Factor Like GTPase 13B
BBS	Bardet Biedl Syndrome
CEBPα	Caat/Enhancer Binding Protein alpha
cko	conditional knock-out
DD	differentiation day
EV	empty vector
Hh	Hedgehog
IFT	intraflagellar transport
kd	knock-down
PPARγ	Peroxisome proliferator-activated receptor gamma
Thm1	TPR-containing Hedgehog modulator 1

References

1. Stephens JM (2012) The fat controller: adipocyte development. PLoS biology 10, e1001436 [PubMed: 23209380]
2. Christodoulides C, Lagathu C, Sethi JK, and Vidal-Puig A (2009) Adipogenesis and WNT signalling. Trends in endocrinology and metabolism: TEM 20, 16–24 [PubMed: 19008118]
3. Kim JY, van de Wall E, Laplante M, Azzara A, Trujillo ME, Hofmann SM, Schraw T, Durand JL, Li H, Li G, Jelicks LA, Mehler MF, Hui DY, Deshaies Y, Shulman GI, Schwartz GJ, and Scherer PE (2007) Obesity-associated improvements in metabolic profile through expansion of adipose tissue. J. Clin. Invest 117, 2621–2637 [PubMed: 17717599]
4. Hildebrandt F, Benzing T, and Katsanis N (2011) Ciliopathies. N. Engl. J. Med 364, 1533–1543 [PubMed: 21506742]
5. Guo DF, and Rahmouni K (2011) Molecular basis of the obesity associated with Bardet-Biedl syndrome. Trends in endocrinology and metabolism: TEM 22, 286–293 [PubMed: 21514177]
6. Girard D, and Petrovsky N (2011) Alstrom syndrome: insights into the pathogenesis of metabolic disorders. Nature reviews. Endocrinology 7, 77–88
7. Qin H, Diener DR, Geimer S, Cole DG, and Rosenbaum JL (2004) Intraflagellar transport (IFT) cargo: IFT transports flagellar precursors to the tip and turnover products to the cell body. J. Cell Biol. 164, 255–266 [PubMed: 14718520]

8. Goetz SC, and Anderson KV (2010) The primary cilium: a signalling centre during vertebrate development. Nat Rev Genet 11, 331–344 [PubMed: 20395968]

9. Mukhopadhyay S, Wen X, Chih B, Nelson CD, Lane WS, Scales SJ, and Jackson PK (2010) TULP3 bridges the IFT-A complex and membrane phosphoinositides to promote trafficking of G protein-coupled receptors into primary cilia. Genes Dev. 24, 2180–2193 [PubMed: 20889716]

10. Fu W, Wang L, Kim S, Li J, and Dynlacht BD (2016) Role for the IFT-A Complex in Selective Transport to the Primary Cilium. Cell reports 17, 1505–1517 [PubMed: 27806291]

11. Nachury MV, Loktev AV, Zhang Q, Westlake CJ, Peranen J, Merdes A, Slusarski DC, Scheller RH, Bazan JF, Sheffield VC, and Jackson PK (2007) A core complex of BBS proteins cooperates with the GTPase Rab8 to promote ciliary membrane biogenesis. Cell 129, 1201–1213 [PubMed: 17574030]

12. Scheidecker S, Etard C, Pierce NW, Geoffroy V, Schaefer E, Muller J, Chennen K, Flori E, Pelletier V, Poch O, Marion V, Stoetzel C, Strahle U, Nachury MV, and Dollfus H (2014) Exome sequencing of Bardet-Biedl syndrome patient identifies a null mutation in the BBSome subunit BBIP1 (BBS18). J. Med. Genet 51, 132–136 [PubMed: 24026985]

13. Lechtreck KF, Johnson EC, Sakai T, Cochran D, Ballif BA, Rush J, Pazour GJ, Ikebe M, and Witman GB (2009) The Chlamydomonas reinhardtii BBSome is an IFT cargo required for export of specific signaling proteins from flagella. J. Cell Biol. 187, 1117–1132 [PubMed: 20038682]

14. Su X, Driscoll K, Yao G, Raed A, Wu M, Beales PL, and Zhou J (2014) Bardet-Biedl syndrome proteins 1 and 3 regulate the ciliary trafficking of polycystic kidney disease 1 protein. Hum. Mol. Genet 23, 5441–5451 [PubMed: 24939912]

15. Xu Q, Zhang Y, Wei Q, Huang Y, Li Y, Ling K, and Hu J (2015) BBS4 and BBS5 show functional redundancy in the BBSome to regulate the degradative sorting of ciliary sensory receptors. Scientific reports 5, 11855 [PubMed: 26150102]

16. Zhang Q, Yu D, Seo S, Stone EM, and Sheffield VC (2012) Intrinsic protein-protein interaction-mediated and chaperonin-assisted sequential assembly of stable bardet-biedl syndrome protein complex, the BBSome. J. Biol. Chem 287, 20625–20635 [PubMed: 22500027]

17. Seo S, Baye LM, Schulz NP, Beck JS, Zhang Q, Slusarski DC, and Sheffield VC (2010) BBS6, BBS10, and BBS12 form a complex with CCT/TRiC family chaperonins and mediate BBSome assembly. Proc. Natl. Acad. Sci. U. S. A 107, 1488–1493 [PubMed: 20080638]

18. Forcioli-Conti N, Lacas-Gervais S, Dani C, and Peraldi P (2015) The primary cilium undergoes dynamic size modifications during adipocyte differentiation of human adipose stem cells. Biochem. Biophys. Res. Commun 458, 117–122 [PubMed: 25637533]

19. Huang-Doran I, and Semple RK (2010) Knockdown of the Alstrom syndrome-associated gene Alms1 in 3T3–L1 preadipocytes impairs adipogenesis but has no effect on cell-autonomous insulin action. Int J Obes (Lond) 34, 1554–1558 [PubMed: 20514046]

20. Qiu N, Cao L, David V, Quarles LD, and Xiao Z (2010) Kif3a deficiency reverses the skeletal abnormalities in Pkd1 deficient mice by restoring the balance between osteogenesis and adipogenesis. PloS one 5, e15240 [PubMed: 21151991]

21. Marion V, Stoetzel C, Schlicht D, Messaddeq N, Koch M, Flori E, Danse JM, Mandel JL, and Dollfus H (2009) Transient ciliogenesis involving Bardet-Biedl syndrome proteins is a fundamental characteristic of adipogenic differentiation. Proc. Natl. Acad. Sci. U. S. A 106, 1820–1825 [PubMed: 19190184]

22. Marion V, Mockel A, De Melo C, Obringer C, Claussmann A, Simon A, Messaddeq N, Durand M, Dupuis L, Loeffler JP, King P, Mutter-Schmidt C, Petrovsky N, Stoetzel C, and Dollfus H (2012) BBS-induced ciliary defect enhances adipogenesis, causing paradoxical higher-insulin sensitivity, glucose usage, and decreased inflammatory response. Cell metabolism 16, 363–377 [PubMed: 22958920]

23. Starks RD, Beyer AM, Guo DF, Boland L, Zhang Q, Sheffield VC, and Rahmouni K (2015) Regulation of Insulin Receptor Trafficking by Bardet Biedl Syndrome Proteins. PLoS genetics 11, e1005311 [PubMed: 26103456]

24. Tran PV, Haycraft CJ, Besschetnova TY, Turbe-Doan A, Stottmann RW, Herron BJ, Chesebro AL, Qiu H, Scherz PJ, Shah JV, Yoder BK, and Beier DR (2008) THM1 negatively modulates mouse

sonic hedgehog signal transduction and affects retrograde intraflagellar transport in cilia. Nat. Genet 40, 403–410 [PubMed: 18327258]

25. Davis EE, Zhang Q, Liu Q, Diplas BH, Davey LM, Hartley J, Stoetzel C, Szymanska K, Ramaswami G, Logan CV, Muzny DM, Young AC, Wheeler DA, Cruz P, Morgan M, Lewis LR, Cherukuri P, Maskeri B, Hansen NF, Mullikin JC, Blakesley RW, Bouffard GG, Gyapay G, Rieger S, Tonshoff B, Kern I, Soliman NA, Neuhaus TJ, Swoboda KJ, Kayserili H, Gallagher TE, Lewis RA, Bergmann C, Otto EA, Saunier S, Scambler PJ, Beales PL, Gleeson JG, Maher ER, Attie-Bitach T, Dollfus H, Johnson CA, Green ED, Gibbs RA, Hildebrandt F, Pierce EA, and Katsanis N (2011) TTC21B contributes both causal and modifying alleles across the ciliopathy spectrum. Nat. Genet 43, 189–196 [PubMed: 21258341]
26. Jacobs DT, Silva LM, Allard BA, Schonfeld MP, Chatterjee A, Talbott GC, Beier DR, and Tran PV (2016) Dysfunction of intraflagellar transport-A causes hyperphagia-induced obesity and metabolic syndrome. Dis Model Mech 9, 789–798 [PubMed: 27482817]
27. Klaunig JE, Goldblatt PJ, Hinton DE, Lipsky MM, Chacko J, and Trump BF (1981) Mouse liver cell culture. I. Hepatocyte isolation. In Vitro 17, 913–925 [PubMed: 6273298]
28. Ni HM, McGill MR, Chao X, Du K, Williams JA, Xie Y, Jaeschke H, and Ding WX (2016) Removal of acetaminophen protein adducts by autophagy protects against acetaminophen-induced liver injury in mice. J. Hepatol 65, 354–362 [PubMed: 27151180]
29. Zhu D, Shi S, Wang H, and Liao K (2009) Growth arrest induces primary-cilium formation and sensitizes IGF-1-receptor signaling during differentiation induction of 3T3–L1 preadipocytes. J. Cell Sci. 122, 2760–2768 [PubMed: 19596798]
30. Dalbay MT, Thorpe SD, Connelly JT, Chapple JP, and Knight MM (2015) Adipogenic Differentiation of hMSCs is Mediated by Recruitment of IGF-1r Onto the Primary Cilium Associated With Cilia Elongation. Stem Cells 33, 1952–1961 [PubMed: 25693948]
31. Gerdes JM, Christou-Savina S, Xiong Y, Moede T, Moruzzi N, Karlsson-Edlund P, Leibiger B, Leibiger IB, Ostenson CG, Beales PL, and Berggren PO (2014) Ciliary dysfunction impairs beta-cell insulin secretion and promotes development of type 2 diabetes in rodents. Nature communications 5, 5308
32. Kraegen EW, Clark PW, Jenkins AB, Daley EA, Chisholm DJ, and Storlien LH (1991) Development of muscle insulin resistance after liver insulin resistance in high-fat-fed rats. Diabetes 40, 1397–1403 [PubMed: 1936601]
33. Kim SP, Ellmerer M, Van Citters GW, and Bergman RN (2003) Primacy of hepatic insulin resistance in the development of the metabolic syndrome induced by an isocaloric moderate-fat diet in the dog. Diabetes 52, 2453–2460 [PubMed: 14514627]
34. Melvin A, O'Rahilly S, and Savage DB (2018) Genetic syndromes of severe insulin resistance. Curr. Opin. Genet. Dev 50, 60–67 [PubMed: 29477938]
35. Dash S, Sano H, Rochford JJ, Semple RK, Yeo G, Hyden CS, Soos MA, Clark J, Rodin A, Langenberg C, Druet C, Fawcett KA, Tung YC, Wareham NJ, Barroso I, Lienhard GE, O'Rahilly S, and Savage DB (2009) A truncation mutation in TBC1D4 in a family with acanthosis nigricans and postprandial hyperinsulinemia. Proc. Natl. Acad. Sci. U. S. A 106, 9350–9355 [PubMed: 19470471]
36. Moltke I, Grarup N, Jorgensen ME, Bjerregaard P, Treebak JT, Fumagalli M, Korneliussen TS, Andersen MA, Nielsen TS, Krarup NT, Gjesing AP, Zierath JR, Linneberg A, Wu X, Sun G, Jin X, Al-Aama J, Wang J, Borch-Johnsen K, Pedersen O, Nielsen R, Albrechtsen A, and Hansen T (2014) A common Greenlandic TBC1D4 variant confers muscle insulin resistance and type 2 diabetes. Nature 512, 190–193 [PubMed: 25043022]
37. Omenetti A, Porrello A, Jung Y, Yang L, Popov Y, Choi SS, Witek RP, Alpini G, Venter J, Vandongen HM, Syn WK, Baroni GS, Benedetti A, Schuppan D, and Diehl AM (2008) Hedgehog signaling regulates epithelial-mesenchymal transition during biliary fibrosis in rodents and humans. J. Clin. Invest 118, 3331–3342 [PubMed: 18802480]
38. Machado MV, and Diehl AM (2018) Hedgehog signalling in liver pathophysiology. J. Hepatol 68, 550–562 [PubMed: 29107151]
39. Finetti F, Paccani SR, Riparbelli MG, Giacomello E, Perinetti G, Pazour GJ, Rosenbaum JL, and Baldari CT (2009) Intraflagellar transport is required for polarized recycling of the TCR/CD3 complex to the immune synapse. Nature cell biology 11, 1332–1339 [PubMed: 19855387]

40. Benzinou M, Walley A, Lobbens S, Charles MA, Jouret B, Fumeron F, Balkau B, Meyre D, and Froguel P (2006) Bardet-Biedl syndrome gene variants are associated with both childhood and adult common obesity in French Caucasians. Diabetes 55, 2876–2882 [PubMed: 17003356]

41. Ritter A, Friemel A, Kreis NN, Hoock SC, Roth S, Kielland-Kaisen U, Bruggmann D, Solbach C, Louwen F, and Yuan J (2018) Primary Cilia Are Dysfunctional in Obese Adipose-Derived Mesenchymal Stem Cells. Stem Cell Reports 10, 583–599 [PubMed: 29396182]

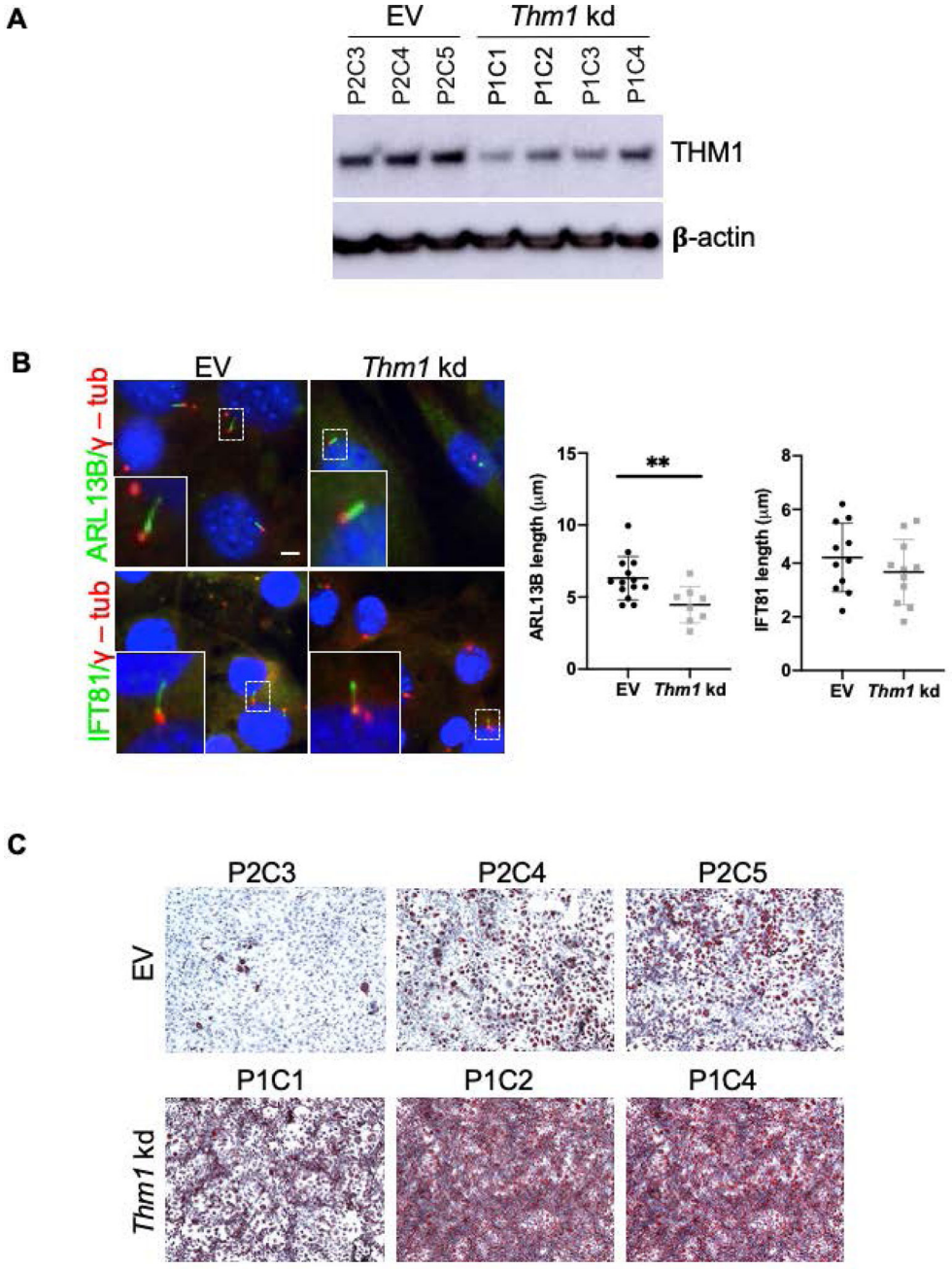

Figure 1. *Thm1* knock-down in pre-adipocytes enhances differentiation.

A) Western blot analysis for THM1 on extracts of EV and *Thm1* kd 3T3–L1 preadipocyte clonal lines. B) Immunostaining for primary cilia markers on EV (P2C3) and *Thm1* knock-down cells (P1C1) with quantification. Graphs represent mean ± SD. Statistical significance was determined by T test. **P<0.01 C) Oil red O staining following adipogenesis assay.

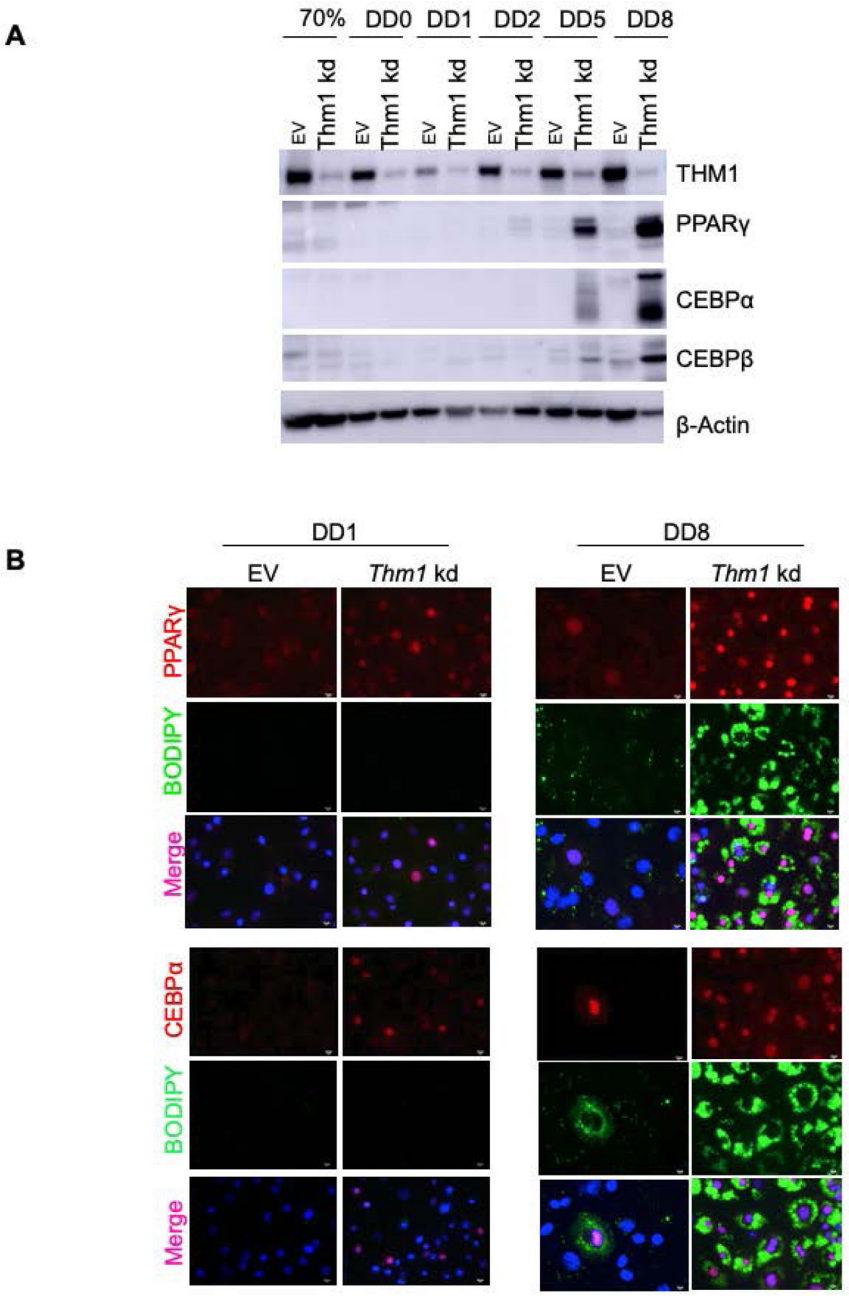

Figure 2. *Thm1*-deficient 3T3–L1 cells show earlier induction of adipogenesis master transcriptional regulators, C/EBPα and PPARγ.

A) Western blot analysis at different differentiation days. B) Immunostaining at DD1 and DD8. Experiments were performed ≥3 times with EV (P2C3) and *Thm1* kd cells (P1C1).

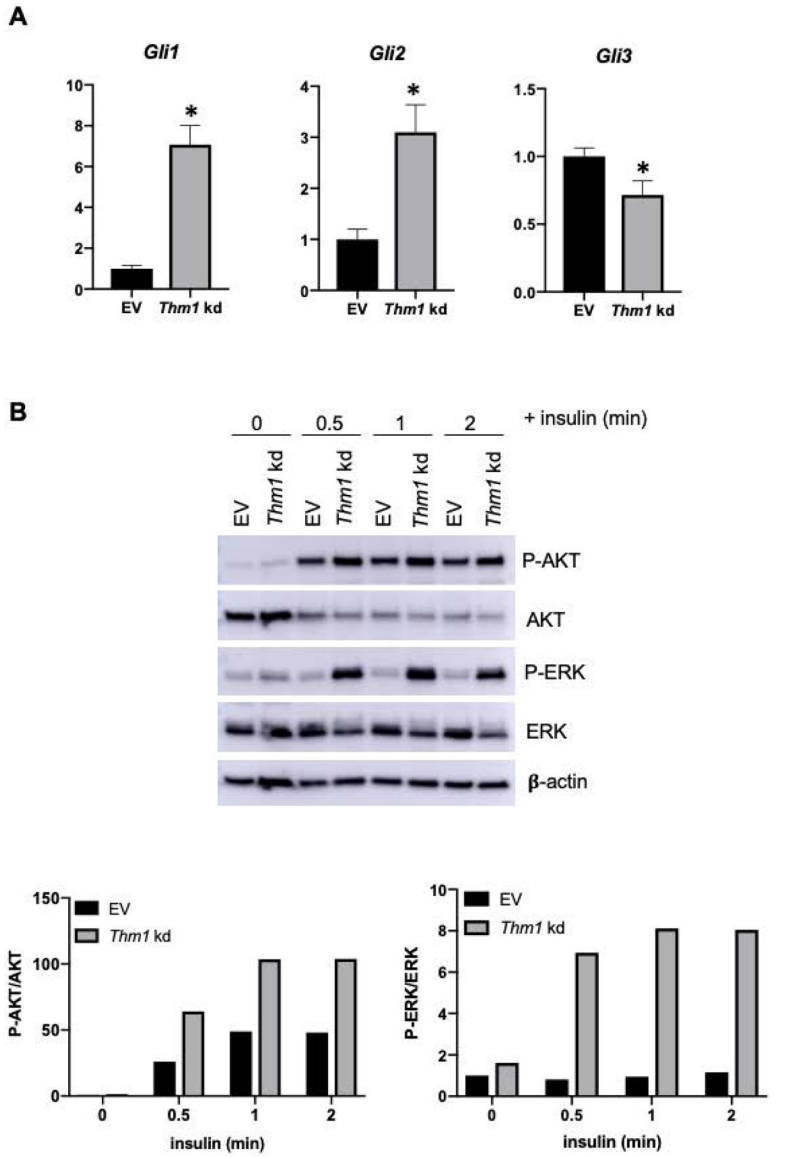

Figure 3. *Thm1*-deficient 3T3–L1 cells are sensitized to insulin signaling.

A) qPCR of pre-adipocytes at DD0. N=5 for EV (P2C3); N=5 for *Thm1* kd (P1C1) B) Western blot analysis of insulin-stimulated pre-adipocytes at DD0 and quantification. Experiment was performed 4 times. Additional experiments are shown in Figure S1.

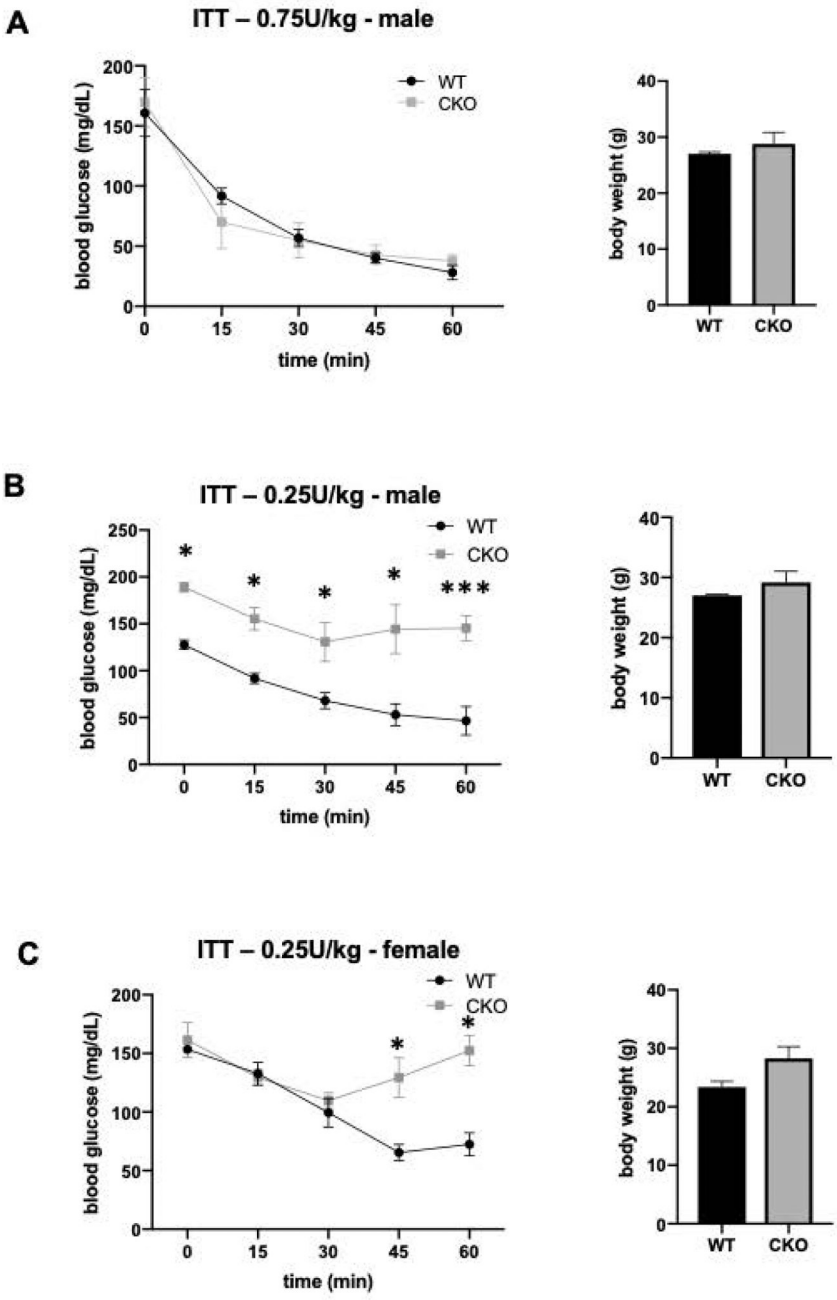

Figure 4. Pre-obese *Thm1* conditional knock-out mice have reduced systemic insulin sensitivity. Insulin tolerance tests and animal weights A) of pre-obese male mice injected with 0.75U/kg insulin; N=3 control; N=3 *Thm1* cko mice; B) of pre-obese male mice injected with 0.25U/kg insulin; N=3 control; N=3 *Thm1* cko males; C) of pre-obese female mice injected with 0.25U/kg insulin; N=3 control; N=3 *Thm1* cko females. Graphs represent mean ± SEM. Statistical significance was determined by T test. *P<0.05; ***P< 0.0005; ****P< 0.00005

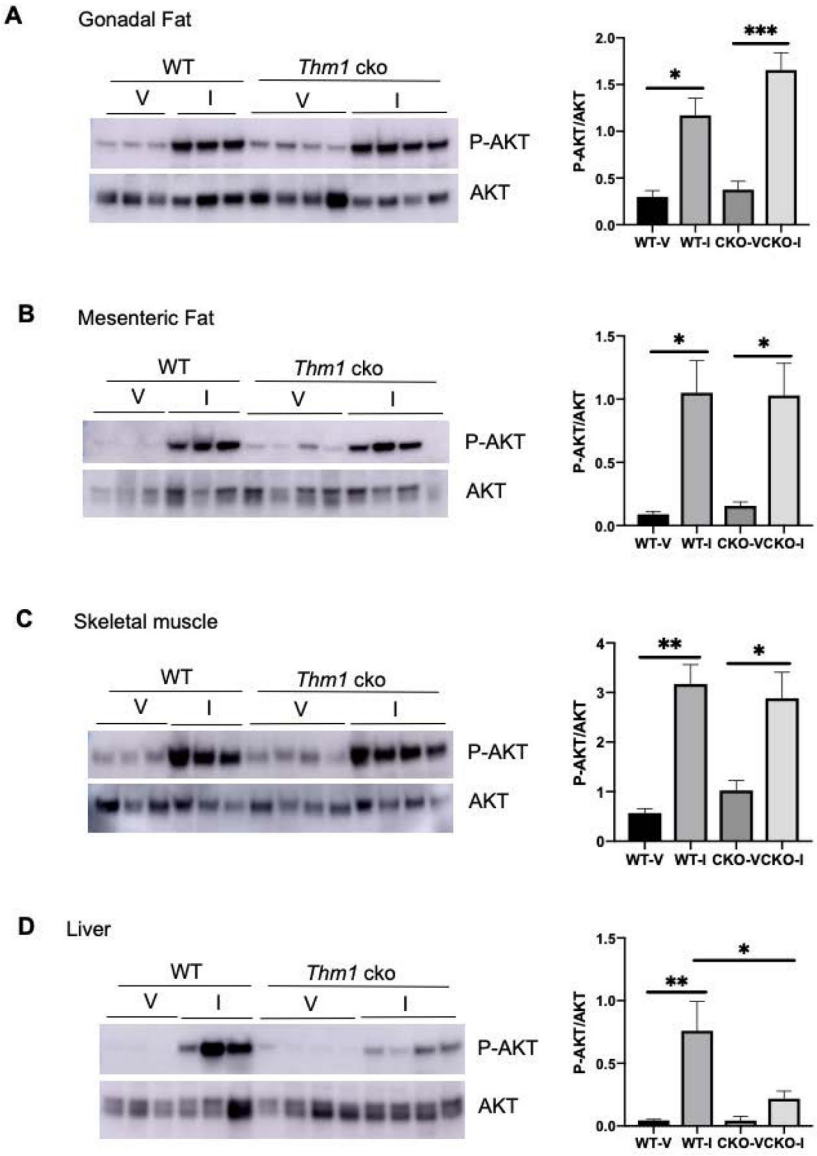

Figure 5. Pre-obese *Thm1* conditional knock-out mice show attenuated insulin response in liver.
Western blot analysis following i.p. injection of pre-obese mice with 5U/kg insulin on lysates of A) gonadal fat, B) mesenteric fat, C) skeletal muscle and D) liver. Graphs show quantification of Western blots. Bars represent mean ± SEM. Statistical significance was determined by ANOVA and Tukey's test. *P<0.05; **P< 0.005; ***P< 0.0005

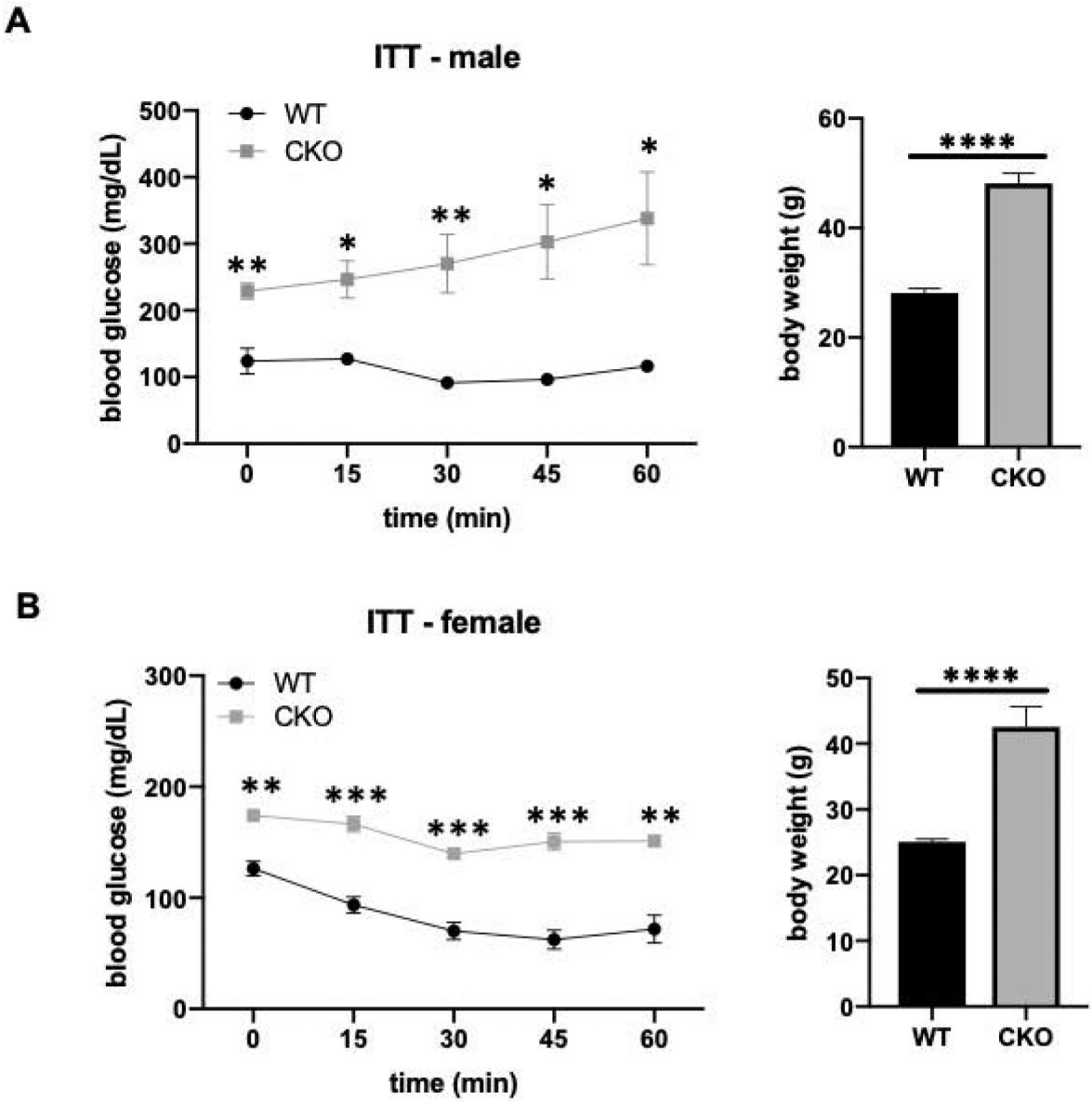

Figure 6. Overweight *Thm1* conditional knock-out mice show systemic insulin resistance.

Insulin tolerance tests (0.25U/kg insulin) and body weights A) of overweight males; N=4 control; N=3 *Thm1* cko males; and B) of overweight females; N=6 control; N=3 *Thm1* cko females. Graphs represent mean ± SEM. Statistical significance was determined by T test. *P<0.05; **P<0.005; ***P< 0.0005; ****P< 0.00005

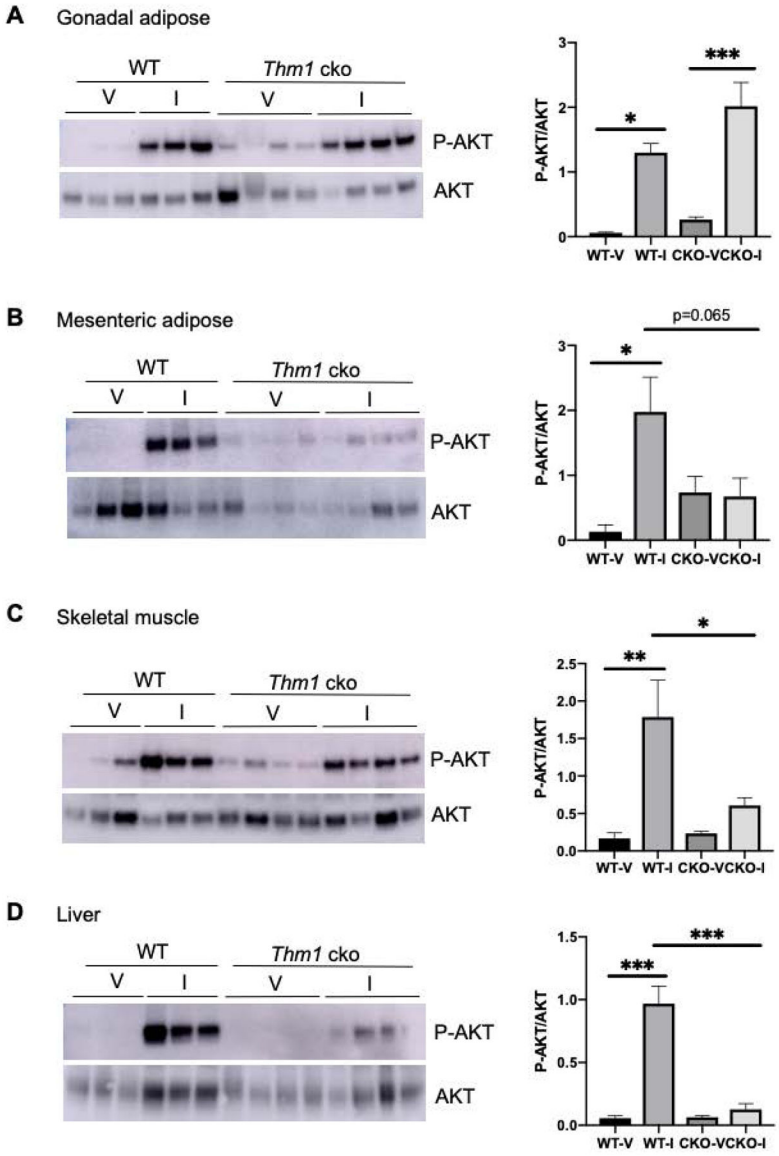

Figure 7. Overweight *Thm1* conditional knock-out mice show attenuated insulin response in liver, skeletal muscle and mesenteric adipose tissue.

Western blot analysis following i.p. injection of overweight mice with 5U/kg insulin on lysates of A) gonadal fat, B) mesenteric fat, C) skeletal muscle and D) liver. Graphs show quantification of Western blots. Bars represent mean ± SEM. Statistical significance was determined by ANOVA and Tukey's test. *P<0.05; **P< 0.005; ***P< 0.0005

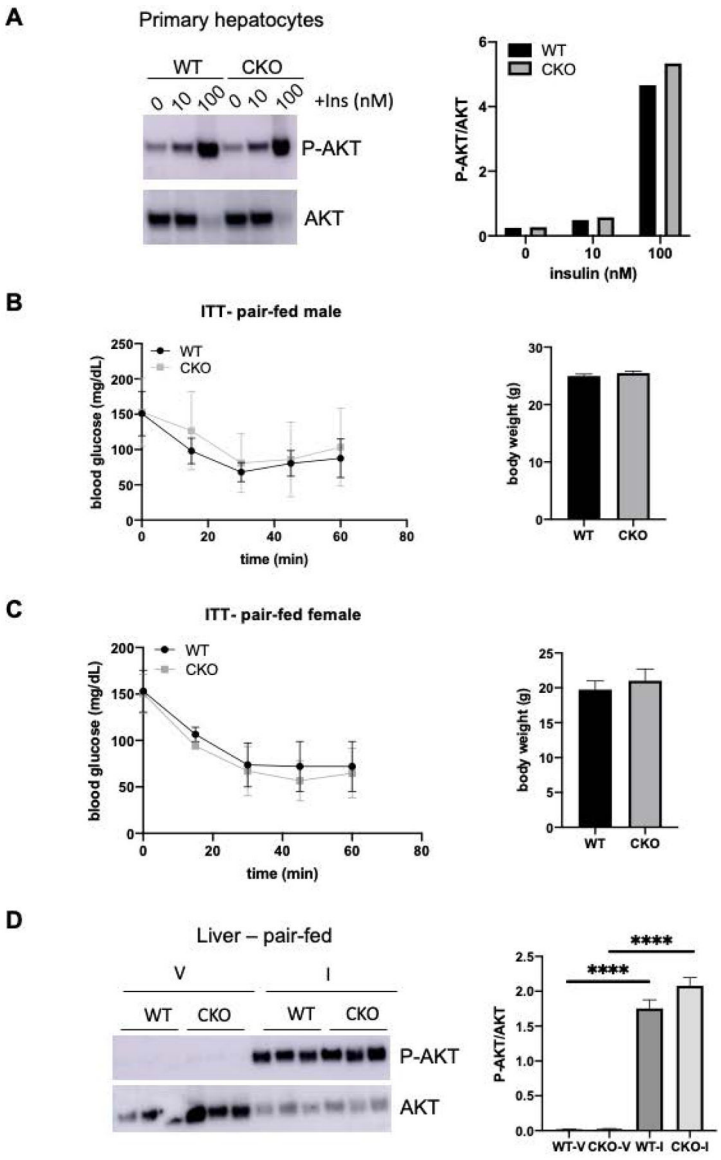

Figure 8. Pair-fed *Thm1* conditional knock-out mice show normal insulin response.

A) Western blot analysis on extracts of primary hepatocytes treated with insulin for 5 minutes with quantification. Shown is a representative experiment of N=2. B) Insulin tolerance tests (0.25U/kg) and body weights of pair-fed males and females. N=3 control; N=3 *Thm1* cko mice. Graphs represent mean ± SEM. C) Western blot analysis on liver lysates of pair-fed mice following i.p. injection of 5U/kg insulin. Graph shows quantification of Western blot. Bars represent mean ± SEM.